Molecular Dynamics Simulations of Enantiomeric Separations as an Interfacial Process in HPLC

Cynthia J. Jameson[1] | Xiaoyu Wang[2] | Sohail Murad[2]

1 Department of Chemistry, University of Illinois at Chicago, Chicago, Illinois

2 Department of Chemical and Biological Engineering, Illinois Institute of Technology, Chicago, Illinois

Abstract

Since chromatographic separation is a dynamic process, with the interactions between the drug and the chiral stationary phase mediated by the solvent, no single interacting structure, such as could be found by minimizing the energy, could possibly describe and account for the ratio of residence times in the chromatographic column for the enantiomeric pair. We describe the use of explicit-solvent fully atomistic molecular dynamics simulations, permitting all the interactions between the atoms constituting the chiral stationary phase, solvent molecules and the drug molecule. This allows us to better understand the molecular dynamic chiral recognition that provides the discrimination which results in the separation of enantiomers by high performance liquid chromatography. It also provides a means of predicting, for a given set of conditions, which enantiomer elutes first and an estimate of the expected separation factor. In this review we consider the use of molecular dynamics towards this understanding and prediction.

1. Introduction

Chromatographic separation of chiral enantiomers is one of the best available methods to obtain enantio-pure substances, [1, 2] but the optimization of the experimental

conditions can be very time-consuming. There have been some attempts to develop a generic separation strategy, with a set of detailed screening steps followed by optimization, [3, 4] but such a strategy would be very expensive to carry out. A practical application of our search for understanding the molecular mechanism for chiral recognition and separation using a chiral stationary phase (CSP) is to be able to provide a computational pre-screening method to find among a set of possible experimental conditions (choice of chiral selector, choice of solvent system, choice of chemical additives or modifiers, pH conditions, column temperature), those optimum set or sets which provide the most favorable separation factors. Many different types of CSPs have been synthesized and commercialized, such as Pirkle or brush types, polysaccharide-based, cavity, ligand exchange. Of all the CSPs available on the market, polysaccharide-based CSPs, especially derivatives of cellulose and amylose, are the most widely used, because of their efficiency, versatility, and durability, [5] but they are also computationally challenging because of size.

By developing computational protocols at the atomistic level that includes the solvent explicitly, a better understanding of the molecular mechanism for chiral recognition can emerge, at the same time, help to reduce the costly experimental trial and error experimental pre-screening steps. The hope is that by running massively parallel MD simulations, the time for a computational pre-screening is limited only by the time it takes to carry out one set of conditions. One could run 100 parallel simulations instead of running 100 HPLC experiments. At the same time, it would be a distinct advantage to have a predictive method that could provide the absolute chirality of the

enantiomer that elutes first, or even choose a set of conditions that permits the desired chiral species to elute first or last.

Early simulation studies of chromatographic separation used a stochastic model of adsorption-desorption behavior of a molecule at a chromatographic interface, using rate constants or residence times, which ultimately were derived from experiments, [6, 7, 8] Pasti et al. [7] have used a stochastic approach to model elution in HPLC as the result of adsorption-desorption processes on the surface stationary phase, leading to peak shapes. We are not concerned with such modeling here. We will focus instead on molecular-level interactions that lead to enantiomeric separation, chiral recognition and enantiomer distinction. The mechanism of chiral recognition has been a long-standing interest in biology and chemistry. [9, 10] Earlier works in atomistic modeling of enantioselection in chromatography have been reviewed by Lipkowitz, [11] and molecular simulation studies of reversed phase liquid chromatography with explicit treatment of solid substrate have been reviewed by Siepmann et al. [12]

2. Earlier models used to understand chiral discrimination

2.1 Three-point model: In order for enantiomers to be chromatographically separated on a chiral stationary phase (CSP), each enantiomer must form transient diastereomeric complexes with the CSP, and the stabilities of these complexes must differ from each other to allow chromatographic separation to occur. The enantiomer that forms the less stable complex will be less retained and hence will elute earlier than will the enantiomer that forms the more stable complex. A number of chiral recognition models have been proposed to account for chiral separation by HPLC; these are often based upon static models such as the three-point interaction rule, i.e., that at least three sites of

interaction must be available to effect chiral discrimination, often referred to as the Easson-Stedman "three-point interaction" model that three simultaneously operating interactions between an enantiomer and the stationary phase are needed for chiral discrimination. [10, 9] It claims that the CSPs should have two hydrogen-bond interactions and one π- π interaction to differentiate the enantiomers; one of the enantiomer-CSP configuration could have three interactions but the other corresponding configuration could only have two interactions due to steric hindrance. Pirkle and Pochapsky [13] described and clarified the *three-point rule*, which has become known as Pirkle's rule, that there must be three simultaneous interactions between the chiral selector and at least one of the enantiomers, and that one of these interactions must be stereochemically dependent. Extension to a 4-contact point interaction model and to a more general criterion based on the differences between the distance matrices of chiral molecules and selectors followed. [14, 15, 16] These are all static models. Despite decades of concerns about the inadequacy of the simplistic three-point interaction model, it is still used for illustrative purposes. [17]

2.2 Molecular docking of enantiomers on a fragment of the CSP in vacuum: By far, the most common explanations of chiral separation have been carried out by simulation of diastereomer formation between a rigid structure of an enantiomer of the analyte and a rigid structure of a fragment of the CSP in vacuum. Molecular docking is generally used to simulate the interaction between the enantiomer pairs and the active site of the selector in order to predict both energy and geometry of selector-analyte binding.[18, 19] At the end of docking calculations, several conformers of the enantiomers are obtained and clustered into several sets. Results are given in terms of the mean binding energy

of the clusters or the mean energy of the most populated cluster; these are used to predict which enantiomer elutes first. The tools first introduced in 1998 by Morris et al. [18, 19] has led to the now commonly used software AutoDock4 and AutoDockTools4. An alternative computational protocol of Gasparrini's called the Global Molecular Interaction Evaluation (Glob-MolInE) [20] involves a conformational search of both isolated selector and analyte; then the automatic systematic rigid docking is run, submitting all the minimum energy conformers within a certain energy window, and finally the rigid dynamic docking is carried out. Unless otherwise noted, molecular docking is carried out in vacuum. Often, only a fragment of the chiral stationary phase is used for docking, for example, only a monomer of a polysaccharide polymer has been used as a representation of the polymers coated on silica support.[21,22] Sometimes a portion of the crystal structure of the polymer is used,[23] e.g., a 6-mer; from the different poses obtained after some number of docking runs; the pose with the lowest energy conformation would be selected.[24, 25, 26, 27] Often, docking techniques are first used to explore a vast conformational space in a short time and scan the possible diastereomeric orientations, followed by geometry relaxation using MD simulations in vacuum or in a uniform dielectric for the few complexes that have been selected. [28] In this approach, MD is used as an *a posteriori* refinement in essentially static models.

3. Molecular Dynamics (MD) simulations as a method of describing the dynamic chromatographic process

Static configurational recognition models overlook the fact that chiral recognition is a dynamic process, in which the structure of CSPs and enantiomers change dynamically in the presence of the mobile phase. MD simulations provide a dynamic atomistic

representation of the interaction between the analyte enantiomers and the chiral selector; thus, a large variety of distribution information can be examined, and averages can be obtained over MD trajectories hundreds of ns long. Where the analyte is fairly flexible, capable of undergoing conformational changes while interacting with the chiral stationary phase, the MD simulations can provide a sampling over these dynamic conformations. A further advantage is that, we can actually test, at will, whether particular chemical modifications to the CSP will enhance the differences in the chiral interactions of the enantiomers with the CSP. Simply increasing the number of CPUs running parallel MD simulations reduces the overall simulation times for large numbers of possible experimental conditions, down to the limit of the time it takes to run a specific one of these conditions. We do need fully atomistic MD; since H-bonding cannot be otherwise well-represented. Particularly for the polysaccharide-based CSPs, we have used MD simulations to provide a molecular level understanding of the dynamic separation process and, for a given set of conditions, for predicting which enantiomer elutes first, and for an estimate of the ratio of residence times or separation factor.[29, 30, 31]

Some questions that can be answered by MD simulations are: Where does the analyte tend to bind around the CSP; do both enantiomers bind to the same or different binding sites? What are the specific intermolecular interactions that are responsible for binding or diastereomer formation? What interactions are responsible for discrimination between enantiomers? What fragment or fragments of the CSP contribute the most to binding, and are these the same ones that contribute to discrimination? What conformations of the CSP are most discriminating? Is there a cooperative effect or

induced fit, i.e., a change in conformation of CSP or analyte or both to enhance binding? What role does solvent play in strength of binding and in selectivity? Of course, all such questions are specific to the CSP, analyte and solvent system. However, with a sufficient number of analytes studied, it may be possible to find commonalities for a given CSP in a given solvent system. For brush-type CSPs of covalently-bonded selectors, other questions such as details of the bonded structure may be answered by MD simulations, such as end-to-end distance of the grafted chain, grafting density, tilt angle, order parameter of the chain backbone, the density profile of the solvent molecules along the normal to the silica surface, etc.

3.1 Factors that need to be considered in designing the simulation system:

Simulations of interfaces present many challenges. Stationary phases are particularly difficult to represent in simulations because they require an atomic level description of the selector, usually a large molecule, along with some approximation of its distribution on the surface and a representation of the underlying solid substrate. There are many options in carrying out MD simulations; for brevity we limit this discussion to atomistic simulations, which comprehensively explore the interactions between the chiral small molecules and the chiral stationary phase. Factors to consider are: First, there is the option of including some representation of the solid support; (a) this could be treated as atomistically dynamic, an amorphous silica slab capped with silanols at the proper distribution of OH types in agreement with experiment for coated types of CSPs, [31] or (b) a single layer of immoveable silicon atoms that represents silica, a rigid structure with surface atoms as tethering points for the selector molecule; [32, 33, 34, 35, 36, 37, 38] the distribution of tethering points may be arbitrary, or regular, or else based on

experimentally estimated grafting density in brush systems, for covalently bonded CSPs. For example, an interface could consist of trimethylsilyl end caps corresponding directly to a truncated selector tether, silanol groups, and selectors covalently attached to a single underlying layer of Si that is stationary throughout the simulation. Alternately, the selector is grafted through an amide linkage to an aminopropyl siloxane-terminated Si(111) wafer, [39] or one could choose (c) not to include the solid support at all, instead compensate for the limited mobility of the polymer coated on solid support with restraining forces, [29, 30] or (d) ignore the solid support and use a freely floating selector molecule or polymer fragment. [29, 30] Second, there is the option of choosing the size of the selector fragment to use in the simulation; (a) for the polysaccharides some have used four 18-mer polymer strands, [31] (b) or a 12-mer single polymer strand, [29] (c) or even shorter strands, such as a 6-mer, [23] tetramer, dimer; use of a monomer (as in Ref. [21] and [22]) would not permit the analyte to feel the groove in the helical polymer structure. For covalently-bonded selectors, the length of the tether is a variable. [33, 34, 35, 36] Third, there is the option of the representation of the solvent system: (a) explicitly atomistic solvent molecules of the appropriate solvent composition can be used, [29, 30] (b) or a continuum model for the solvent with variable dielectric constant adjusted for the composition,[40, 41, 42, 43, 44, 45] or (c) vacuum. [46, 47, 48] Fourth, there is the option of keeping some parts of the system rigid to increase the efficiency of the MD runs. This has been done in several simulations. For example, since aromatic rings have strong force constants that maintain the bond lengths, the symmetry, and also the planar geometry of the ring, Cann et al. have carried out simulations in which the rings of the selector molecule are treated as rigid units; that is, their translation and rotation is

consistent with the forces on the atoms within the unit; but the relative atomic positions within the unit do not vary with time. [32] In this case, intramolecular potentials within the rigid unit are omitted since these will not change with time, while the rigid unit atoms still interact with atoms outside the unit; and are also involved in intramolecular potentials that include other atoms. In the case of the Whelk-O1 selector, MD simulations by Cann et al. have kept both the dinitrophenyl and the tetrahydrophenanthrene group as rigid units. [33] Finally, the choice of force field for various components of the physical system is an important factor. Some simulations have used AMBER and its GAFF library [29, 30, 31] for all components except the silica slab; some have used different force-fields for different components of the system, [33] for example, a combination of CHARMM, OPLS, and Siepmann's TraPPE-UA model.

In doing MD simulations, the starting configuration for the trajectory over which data analyses are carried out is very important because trajectories lasting no more than several hundred nanoseconds up to microseconds are the typical limits in practice for fully atomistic simulations of large systems. For this reason, many practitioners start with a proposed long-lived configuration and then permit the system to explore other configurations over the period of the trajectory. However, this introduces a bias that may affect the results obtained in the data analyses, which may skew the conclusions. For example, many MD simulations of chiral interactions between enantiomers and CSP fragments start from an energy-minimized docked complex, in vacuum, in a continuum solvent of fixed dielectric constant, or in an equilibrated explicit solvent box. With this as starting point, the MD trajectory may not be sufficiently long to permit the system to provide an accurate distribution of configurations or average properties. Also, this would

not permit the correct mechanism for chiral recognition in those cases where solvent is hydrogen-bonded to the selector, and the analyte has to displace the solvent molecules in order to be recognized. The experimentally known elution order for the enantiomers may bias the very early stages of setting up the calculations.

Here are some possible pitfalls. (1) Biasing the starting configuration, as mentioned above. It is better to do an unbiased MD simulation, i.e., without starting the analyte in a pre-determined binding pose in the CSP structure. (2) Truncating the size of the selector is a common strategy, particularly for a polymeric selector; there are possible artifacts from end effects. (3) Ignoring the solid support altogether could misrepresent the nature of the interfacial approach and recognition. (4) Results may depend on the size of the simulation box; size is sufficiently large if results do not change when size is increased. Often, this test is not carried out.

3.2 It is important to include explicit solvent molecules: How does using implicit solvent do better than in-vacuum simulations? As solvent polarity is systematically changed from non-polar to polar solvents, it has often been "observed" that electrostatic interactions tend to increase in nonpolar (low dielectric) solvents; but decrease in more polar (high dielectric) solvents. Of course, it is not even necessary to carry out MD simulations to expect this trend, with the dielectric constant in the denominator in the Coulomb term that is used in MD simulations to describe electrostatic interactions, the magnitude of electrostatic contributions is turned down uniformly by increasing ε from 1 to various values up to 80. Turning down the electrostatic interactions changes the dynamics, as the van der Waals terms then provide a larger fraction of the interactions, leading to entirely different dynamics at close range. On the other hand, solvation or

desolvation events and their effects can only be investigated by using explicit solvent molecules. Also, solvent molecules can hydrogen-bond with the selector, thus, have to be displaced by an approaching enantiomer. It was originally assumed that differential solvation of the competing diastereomeric complexes is of minor importance in chiral discrimination, but this turns out not to be the case, as has been observed when the same analyte is studied in more than one solvent system.

The composition of the mobile phase can have a crucial effect on chiral recognition because it can affect the structure of the chiral selector and the enantiomer. The experimental chromatography literature is replete with indications that the mobile phase could play a role in chiral separations. For example, from recent experimental studies, it has been observed that simply changing the mobile phase can have a significant effect on the separation of chiral drugs; in particular, the ADMPC polymer, exhibits a change in structure when the mobile phase is switched from methanol to hep/IPA or acetonitrile solvent (see Section 6.3). Studies using solid state NMR have already shown that hexane, an often-used component in a binary mobile phase, becomes incorporated into the structure of the CSPs. [49] In the same study, changing to a polar solvent was found to change the structure of the CSPs by affecting its intra- and inter-molecular hydrogen bonds. Therefore, inclusion of explicit solvent molecules is critical in MD simulations to provide a realistic representation of the structural behavior of the CSPs and the enantiomers and their mechanism of interactions with each other. Certainly, the solvent stratification that occurs in mixed solvent systems, observed in MD simulations by Cann et al., [33, 32, 38] and also by others, [29] can only be described by explicit solvent. Implicit solvent MD can represent the average dielectric constant of

such solvent mixtures, but only explicit solvent MD can reveal the non-uniform solvent distribution. Local solvent environments can have effects on the chiral recognition that cannot be duplicated by MD in implicit solvent.

There is extensive literature on rule-of-thumb criteria for chiral discrimination via interactions of specific functional groups or motifs on the racemate with those on the chiral selector.[9, 50, 51] But, as seen above, previous models are static rather than dynamic, and often do not include explicit solvent effects, whereas chiral separation methods, such as chromatography, are dynamic processes, and are known experimentally to change magnitudes of separation factors, even reverse the elution order, merely with a change in solvent composition. In our quest for a better understanding of the molecular mechanism for chiral recognition and separation, we need to consider both the dynamic nature of the process and the important role of the solvent system.

4. MD studies on covalently bonded selectors

Most MD simulations of HPLC have been carried out for reversed phase liquid chromatography (RPLC), where the bonded phase consists of molecules bonded to the solid support with tether chains of various lengths. We mention some examples below. For the so-called brush-type CSPs, where the selector molecules are covalently tethered to the inner surface of the pores in the silica, neither the composition nor the density of the solvent in contact with the stationary phase in a nanometer-scale is known *a priori*. This may be different from the bulk mobile-phase composition, since it is experimentally well known from adsorption in nanoporous materials that the liquid

composition inside the pores is different from that of the bulk. For mixed solvents, like n-hexane with ethanol, this is particularly relevant.

4.1 Preparing the interface. Solvent effects on covalently-bonded selectors:

Siepman et al. [12] have reviewed MD simulations with explicit treatment of the solid substrate, i.e., the surface of the porous silica particles, the bonded chains, and the mobile phase and analyte molecules. For molecular simulations with the retention characteristics typical of an RPLC system, they find that a chain coverage of about 2.9 $\mu mol/m^2$ or higher combined with a chain length of 8 or longer suffices. They conclude, illustrated by simulations capable of high precision and accuracy, that the retention mechanism is very complex at the molecular level, so that generalizations cannot be reliably made that apply to most samples and reversed phase systems. These methods and results for achiral separations, with respect to grafting densities, chain alignment, solvent density profiles near the substrate and interface regions, are enlightening also with respect to enantiomeric separations, e.g., their simulations in which a chiral selector is covalently tethered to a planar slit pore solid support consisting of tertramethylsilane end caps, with no silanols on the surface. [12]

Cann et al. have carried out MD simulations of solvent effects on covalently-bonded selectors, in particular PEPU (N-(1-phenylethyl)-N'- 3-(triethoxysilyl)propyl-urea), [52, 53] DNB-leucine ((R)-N-(3,5-dinitrobenzoyl) leucine), DNB-phenyl glycine ((R)-N-(3,5-dinitrobenzoyl)phenylglycine) for solvents of variable composition, [32] proline-based selectors with variable numbers of proline moieties in the same mixed solvents, [37, 39] 1-(3,5-dinitrobenzamido)-1,2,3,4-tetrahydrophenanthrene or Whelk-O1 in n-hexane/2-propanol, water/methanol, and a

supercritical solvent of CO2 and methanol. [33] Their studies describe the detailed nature of the interface for these types of selectors in the solvent systems. In particular, they discover that changes in the alcohol concentration alters the preferred orientation of the selectors. [32]

4.2 MD simulations of chiral analytes on Whelk-O1 selectors: Cann and co-workers have conducted MD simulations to characterize the Whelk-O1 chiral stationary phase (Pirkle columns). The Whelk-O1 CSP is based on 1-(3,5-dinitrobenzamido)-1,2,3,4-tetrahydrophenanthrene molecules covalently tethered to the silica solid support via a short alkyl tether and a siloxyl group, and assumed to be in a brush form along the inner surface of the pores of silica beads. First, they carried out MD studies on the solvation of the Whelk-O1 chiral stationary phase. [33] In their studies, typically, the selectors, trimethylsilyl end caps, and silanol groups are covalently attached to a single underlying layer of Si atoms that remains stationary throughout the simulation. This layer defines the boundary of the interfacial system, and it is meant to provide a minimal representation of the underlying substrate. [32, 36, 54] Two such surfaces constitute the simulation box top and bottom. To achieve the correct solvent density (e.g., 2-propanol) in the simulation box, they account for the volume of the selectors, end caps, and silanol groups to set the distance between the Si surfaces. Then, the bulk density in the center of the simulation cell is examined during the simulation to ensure that it is within 5% of the experimental density. Then, they carried out MD studies of chiral recognition of styrene oxide and stilbene oxide, [34] and again, together with eight additional analytes in n-hexane. [35] From a comparison of overall docking frequencies for S and R enantiomers, they calculated separation factors, based on Eqn. (1) (see below).

$$\alpha = \frac{K_R}{K_S} = \frac{\langle N_R\rangle_{docked} / \langle N_R\rangle_{undocked}}{\langle N_S\rangle_{docked} / \langle N_S\rangle_{undocked}} = \frac{\langle N_R\rangle_{docked} / [8-\langle N_R\rangle_{docked}]}{\langle N_S\rangle_{docked} / [8-\langle N_S\rangle_{docked}]} \quad (1)$$

where $\langle N_R\rangle_{docked}$ and $\langle N_S\rangle_{docked}$ are the average number of docked R and S enantiomers, respectively. The number of undocked enantiomers is calculated by the difference in the total number of each enantiomer in the simulation box, e.g., 8 in their simulations, and the average number of docked enantiomers. They have written Eq. (1) for the case where R is retained (S elutes first). Experimental definition of the separation factor is for a value always greater than 1, thus, requiring no experimental knowledge of which of R or S elutes first. Analysis of analyte-selector complexes identified four distinct docking arrangements: The most frequent mode consists of an H-bond with the amide H and a π-π stack of the analyte ring with the dinitrophenyl ring of the selector; other modes include H-bonds with the amide oxygen, or H-bonds with the nitro oxygens, or π-π stacking with the phenanthryl group.

One of the advantages of MD simulations is that it is possible to make chemical modification to functional groups of the selector in *in silico* experiments, to investigate differences in the results. From such simulations, a rational optimization of the selector system may be possible. Cann et al. carried this out for the Whelk-O1 chiral stationary phase using MD simulations and found that chemical modifications with specific goals, such as to block the docking of the least retained enantiomer to enhance selectivity, can end up with complex consequences. [36] This further proves the utility of MD simulations; a simple chemical modification that an experimentalist would consider as clear cut with respect to its consequences, turns out to not quite lead to expected results.

4.3 MD simulations of chiral analytes on proline-type selectors: Cann et al. have also carried out MD simulations of chiral separations on proline-based chiral stationary phases. [37, 38, 54, 55] An example of their simulation box is shown in Fig. 1 with the TMA-(Pro)6-N(CH3)-tether chiral stationary phase interacting with the enantiomers of α-methyl-9-anthracenemethanol in the presence of a n-hexane/2-propanol solvent. [38] In the latter study, they find that having tert-butyl end groups with an ether linkage rather than directly attached to the C=O of the diproline chiral selectors made a difference in the accessibility of the analyte to the selector, i.e., more accessible when the configuration is more extended via hydrogen bonding to the solvent, more pronounced in 70/30 water/methanol than in 70/30 n-hexane/2-propanol.

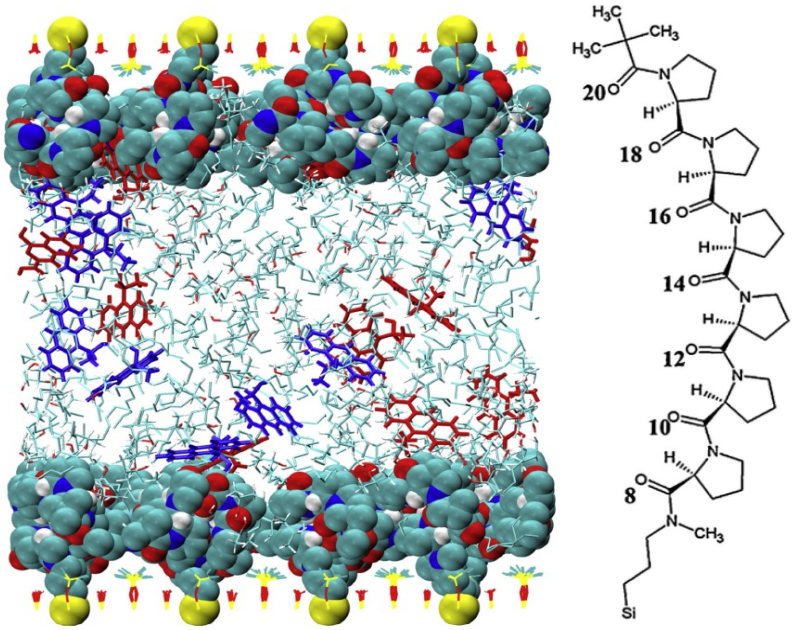

Figure 1. A snapshot from the simulation of the TMA-$(Pro)_6$-$N(CH_3)$-tether chiral stationary phase interacting with the enantiomers of α-methyl-9-anthracenemethanol in the presence of a n-hexane/2-propanol solvent. The hexaproline selector (formula on

the right) is shown in solid atom representation. The Rand S enantiomers are shown in blue and red, respectively. Reproduced with permission from Ref. **38**.

From further MD simulations on this system, they predicted separation factors from hydrogen-bonding counts for 6 different analytes under normal phase elution conditions (70/30 *n*-hexane/2-propanol), derived from MD simulations on a model surface consisting of 16 polyprolines, 64 silanol groups, 48 trimethylsilyl end-caps and 128 fixed Si atoms. The theoretical study was performed by considering the effect of two different mobile phases, namely *n*-hexane/2-propanol, as a nonpolar mixture, and water/methanol, as polar solvent, on chiral recognition. [38]

5. MD studies of chiral molecules interacting with cyclodextrins

Cyclodextrins are composed of 5 or more α-D-glucopyranoside units linked 1-to-4, as in amylose, providing a fairly rigid and well-defined hydrophobic cavity and hydrophilic rims. Starting from the middle 1980s, a large number of cyclodextrin-based CSPs have been designed and used for enantio-separation in HPLC. Recent developments focus on two aspects: functionalization of the CD skeleton and the immobilization on a solid support. [56, 57, 58, 59, 60, 61] In cyclodextrin, the inner circumference of the cavity is lined with hydrogen atoms or glycosidic oxygen bridges and hence has low polarity that favors the attachment of lipophilic molecules; while the hydroxyl groups on the outer surface makes them hydrophilic. To customize the selectivity properties of the molecule, the hydroxyl groups have been substituted using other functional groups. MD studies of chiral analytes interacting with cyclodextrin and its functionalized family of molecules have so far been largely limited to simulations in vacuum only, [62] or in a continuum solvent with a variable dielectric constant parameter.

[40, 41, 42, 43, 46] MD of enantiomers in cyclodextrin in explicit water molecules have also been carried out, but unless done for sufficiently long simulation times, water molecules may not even have the opportunity to make their way inside the cup, as when simulation times are 10 ns or less. In a 50 ns trajectory, the first water molecule goes into the cup only after 22 ns. [63] United atom MD simulations of ibuprofen enantiomers in β-cyclodextrin in the presence of explicit methanol molecules show rather different results compared to MD simulations in vacuum; methanol molecules tend to occupy the majority of possible hydrogen bonding sites. [64]

Cyclodextrin chemically anchored to silica support has been modeled recently. [65] The authors synthesized a CSP with the inverted cup orientation by anchoring mono(2^A-azido-2^A-deoxy)-β-CD (attachment at the large mouth of the cup) onto alkynyl silica via click chemistry, the analogous method by which they previously produced the normal cup orientation using mono(6^A-azido-6^A-deoxy)-β-CD (attachment at the small mouth) (see Fig. 2), and tested both CSP types with a series of isoxazolines and flavonoids as analytes.

Chromatographic results for normal orientation and inverted cup were compared; different drugs have different separation effectiveness in the two different complexing directions. This is an interesting observation when considered with respect to the selectivity of free CD in solution. MD simulations were carried out using NAMD and the CHARMM force field, an explicit water/methanol 50/50 by volume. In the simulation, all glycosidic oxygens were confined to their initial positions, thereby maintaining the cup orientation and position during the simulation. Absolute free energies were calculated

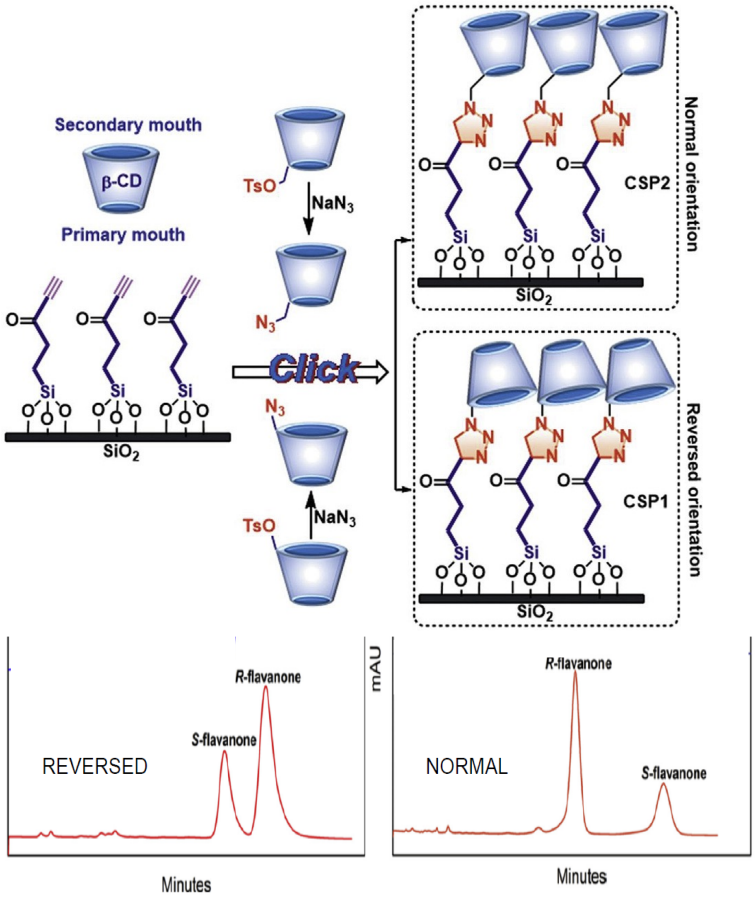

Figure 2. Anchoring β-cyclodextrin to silica to produce chiral stationary phases with either complexing direction: CSP2 (normal orientation) and CSP1 (reversed orientation). Experimental data showing reversal of elution order and change in magnitude of separation factor. Reproduced with permission from Ref. **65**.

from the MD simulations, providing free energy profiles (Potential of Mean Force), see Section 7.4, thereby providing association free energies and association equilibrium constants for each enantiomer, for both complexing directions. [65]

6. MD simulations of chiral recognition using polysaccharide CSPs

6.1 The structure of polysaccharide-based CSPs: Although a large number of chiral stationary phases have been used, [66, 67] the efficiency and wide applicability of the polysaccharide-type chiral stationary phases have led to their wide usage. [68, 69] In

applications, the polysaccharide selector is coated on a solid support, or else covalently bonded to it. A recent overview summarizes the application of polysaccharide-based chiral stationary phases for separation of enantiomers in HPLC, with special emphasis on practical aspects such as a discussion of the optimization of polysaccharide-based chiral selectors, their attachment onto the carrier, and the optimization of the support, and the optimization of the separation of enantiomers based on various parameters such as mobile phase composition and temperature.[70] Polysaccharide column screens seem to provide the best first-tier approach to finding chiral recognition conditions for stationary phases;

The structure and the chiral recognition mechanism of the polysaccharide-based CSPs, have been extensively investigated.[47, 71,72] The structure of one typical example of polysaccharide-based CSPs, often used as the model system, is amylose tris(3,5-dimethyphenylcarbamate) (ADMPC) has been investigated using different experimental techniques, including solid state nuclear magnetic resonance spectroscopy (NMR), [73] NMR in solution using the 2D Nuclear Overhauser Enhancement (NOESY) technique, [74] vibrational circular dichroism (VCD), [75] attenuated total reflection infrared spectroscopy (ATR-IR), and x-ray diffraction. [47] Yamamoto et al. [74] reported that ADMPC possesses a left-handed 4/3 helical structure in chloroform, while Ma et al. [75] used VCD measurements, which also suggested a left-handed helical structure. Similar conclusions were drawn by Wenslow and Wang using solid state NMR. [76] In the helical structure of ADMPC deduced from these observations, the glucose rings are regularly arranged along the axis; the carbamate groups are located inside the grooves of the polymer, while the phenyl groups are located outside the polymer chain. The structure

of the side chain has also been studied and reported by Kasat et al., [77] that it has a planar conformation.

6.2 MD of chiral interaction with polysaccharide-based CSP without explicit solvent: In combination with NMR experiments, Ye et al. [45] used implicit-solvent MD simulations to study the interaction between a 12-mer of ADMPC with a fixed backbone and the enantiomers of *p*-O-tert-butyltyrosine allyl ester which were placed in the groove of ADMPC at the beginning of the simulation. Pair distribution functions generated from the simulations agree well with 2D NOESY spectra. However, the fixed backbone structure and the placement of the enantiomers in the groove might also have caused some artifacts that could affect the results from the 2 ns simulation. Furthermore, implicit solvent simulations do not consider possible local contributions of solvent molecules to the configuration energy. Similar MD simulations have been reported by Kasat et al., [47] which were also conducted on a system containing ADMPC with fixed backbone structure in the absence of solvent molecules. Other polysaccharides coated on silica support have been more recently studied by MD. Hu et al. [44] carried out MD simulations of 11 various imidazoles and a 12-mer cellulose tris (4-methylbenzoate) (Chiralcel OJ) in continuum solvents of various dielectric constants. Starting with the analyte inserted into particular grooves in the 12-mer, they carried out relatively short 100 ps production runs and collected interaction energies every 10 ps. They predicted elution order from mean interaction energies. However, the very short trajectories, the use of implicit solvent, and the wide range (12-20 kcal mol^{-1}) of calculated interaction energies, compared to small differences (3-4 kcal mol^{-1}) in the mean interaction energies for S versus R, point to a need for more comprehensive analysis.

6.3 MD using a single polymer strand in the solvent system: Using a soluble (in chloroform) short (12-mer) ADMPC, it had been possible to use solution NMR to characterize the structure and also to use NOESY experiments to observe cross peaks that appear for H-H short-distance (less than 5 Å) interactions between an H on the analyte and an H on the ADMPC. [78] Since the hydrogens are uniquely assigned in the NMR spectrum, it was possible to deduce accurately from the NMR experiment the spatial arrangement of the analyte on the 12-mer that is consistent with the experimental distances. MD simulations (2 ns, starting from energy-minimized structures) provided two-body distribution functions, in which the r_{HH} corresponding to the first peak correlated very well with the intensities of the cross peaks which are an NMR measure of these distances. This early work was the basis for our assumption that a 12-mer would be a sufficiently long polymer strand to represent the ADMPC chiral stationary phase in fully atomistic MD simulations in explicit solvent that could provide atomic level details of chiral recognition events for both enantiomers. We hoped that the snapshots could provide MD metrics (e.g., various averages over the length of a trajectory) that could be used to predict not only which enantiomer would elute first, but also provide ratios of MD metrics that would correlate well with separation factors. [29, 30] Looking back, it turns out that Ye et al. had chosen an analyte that was most likely to succeed, i.e., D and L O-tert-butyltyrosine allyl ester, having a separation factor α= 16 on ADMPC. The very strong binding of the L enantiomer permitted the NMR experiment to provide sufficient NOEs for quantitative work.

The MD methodology we used is described in Ref. 29-30. It was more efficient to first equilibrate the ADMPC 12-mer with the solvent in 100 ns, and then introduce the

drug for running the simulations for producing averages. A single representative structure of ADMPC is generated in each of the three solvent systems, the most populated backbone structure in three solvent systems: heptane/IPA (90/10), methanol and acetonitrile. [29, 30] Each simulation was carried out for at least 100 ns. Once this was done, the starting equilibrated polymer in solvent was used as an initial ADMPC configuration for all simulations involving different drugs in the same solvent system. Statistical analysis of the trajectories used Ambertools, VMD, NAMD, and in-house scripts. A probability map of the dihedral angles can be obtained from a 40-60 ns simulation after equilibration of the ADMPC polymer in the solvent. This map is analogous to the Ramachandran plot used in describing the secondary structure of polypeptides. [79] The maps show that the ADMPC average configuration in each of the different solvent systems provides a different landscape for the chiral analyte to interact with, since the side-chains assume different distributions of orientations about the backbone when the glycosidic angles change their values. The observed differences in the (φ, ψ) maps for amylose tris(3,5-dimethylphenyl carbamate) suggest the basis for finding modified separation characteristics of a CSP when choosing different solvent systems for a given racemate.

Despite the beautiful agreement with NOESY results in the work of Wirth et al. [78], we found that using a freely floating model of the 12-mer did not generally lead to reliable discrimination when tested with 10 different enantiomeric pairs. Thus, we needed to mimic the restricted motion of the polymer coated on silica surface; otherwise the polymer was insufficiently discriminating in H-bonding and in ring-ring interactions with the analyte. In practice, the polymers are coated on the solid support at a sufficient

coverage so that no free silanols are exposed. Therefore, the degrees of freedom of the polymer are restricted by the silica support and the polymers next to it on the surface. To mimic these conditions, we applied a weak restraining harmonic potential to every atom of the 12-mer; all atoms are still dynamic, but the cavities for close approach of analyte are very regular and consistent in free volume available to the enantiomers; this situation may be more typical of very long polymers laid down on the silica support. We used each enantiomer of 10 analytes shown in Fig. S1 of Supplementary Material, for which experimental data is available, to test this model.

When H-bonding dominates the interactions between a chiral analyte and a selector, hydrogen-bonding counts have often been used as a surrogate for numbers of enantiomers docked; in choosing our metrics we are attempting to go beyond that by including lifetimes in the analysis. We considered six possible MD average quantities associated with H-bonding events (defined in the Supplementary Material) that could be expected to correlate with the elution order and with the value of the separation factor. For a specific donor-acceptor pair, the lifetime is defined as a time period when the hydrogen bonding structure remains present consecutively in the trajectory.

We examined the results for these 6 metrics for individual H donor-acceptor pairs to discover whether the same ones, or different ones, dominate for both enantiomers. [30] The combined results for the restrained 12-mer (averages or maximum values) are shown in Table S1 in Supplementary Material, where the ratios S/R for each of the 6 possible MD metrics are given for each enantiomeric pair shown in Fig. S1. These values are to be compared with the experimental ratio of the retention times (S/R) for the enantiomers of the drug in the given solvent system. For ambucetamide and

etozoline, where only the value α has been reported, we display the experimental α value and its reciprocal as possible values for the experimental ratio S/R. Each of these possible metrics has been plotted against the experimental separation factor (we excluded valsartan, where we did obtain the correct elution order, but the metrics ratios were extremely large. Also, for the purpose of finding the correlation coefficients, we assigned the elution order to be the same as found from MD for the two drugs (ambucetamide and etozoline) for which the absolute chirality of the first eluted enantiomer is still unknown experimentally, but our MD results provide the same prediction across the board for all metrics for these two drugs; therefore, we consider it very likely that we have the correct MD prediction of elution order in these two cases. The elution order is predicted correctly for all drugs except thalidomide. The best correlation coefficients for the restrained single strand polymer in solution were for metrics based on the *maximum lifetimes*; that is, both the average of the individual maximum lifetimes for each donor-acceptor partner and the overall maximum value.

In contrast, an unrestrained free-floating ADMPC 12-mer is not an acceptable model; the H-bonding results were much less consistent, and the distribution maps of orientation angles in ring-ring interactions also showed lack of discrimination; indicating that the unrestrained short polymer in solution may be far too mobile to present a consistent landscape for the approaching enantiomers.

Using *ad hoc* restraints on a 12-mer of ADMPC in order to mimic the restricted motion of the polymer coated on silica, was expedient, but unsatisfying. We did find the correct elution order in all but one case, thalidomide. The model did provide the correct relative order of separation factors using two H-bond lifetimes metrics, with correlation

coefficients 0.863 and 0.876, but the linear plots did not have slopes of unity that one expects from ideal correlation plots. Furthermore, in the case of valsartan, we did have the correct elution order, but one enantiomer exhibited too few H-bonding events, leading to an absurdly high separation factor. All these point to the necessity of finding a better model, despite the successes of this one.

6.4. MD using multiple polymer strands coated on amorphous silica: We developed a much more realistic model consisting of multiple polymer chains on an amorphous silica surface, [31] with the following features: (a) The presence of adjacent polymers is included, thus permitting polymer chain-chain interactions, and also permitting simultaneous interaction of an enantiomer with more than one chain. (b) There is no *ad hoc* partial restraint on the atomic motions as was used previously. (c) The atomistic effects of the amorphous silica solid support on the structure and dynamics of the polymer are included. (d) With the solid support included, the interaction regions presented by the ADMPC to an enantiomer becomes limited, permitting approach not from all radial directions from a single chain; rather, approach is only from the face away from the silica. (e) A further improvement is the use of four 18-mer chains extracted from a solvent-equilibrated 20-mer, instead of a single 12-mer chain. (f) We considered parallel and antiparallel arrangements of the helical strands: (*aaaa, aabb*, *abba*, *abab*). With this model we can understand the role played by the solid support. Fig. 3 summarizes the procedure which is described in detail in Ref. 31.

A typical snapshot of our simulation system is shown in Fig. 4. The backbones of the ADMPC appear quite regular. On the other hand, the side groups are clearly quite mobile. We tested our model with four racemates: benzoin and valsartan in hep/IPA,

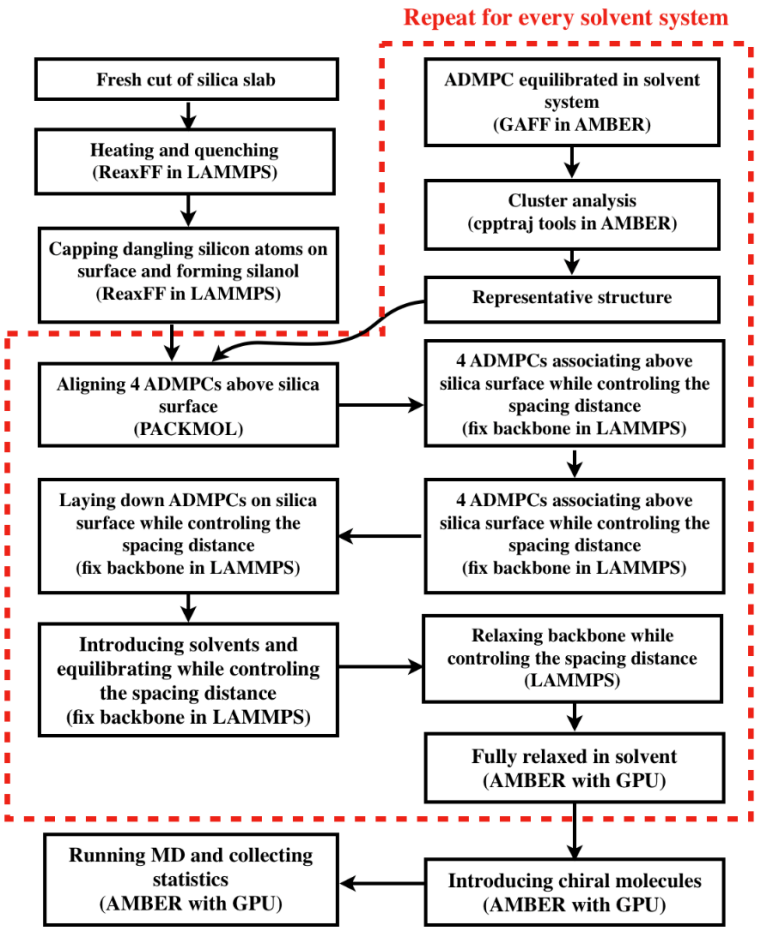

Figure 3. In the red box is the flow chart for preparing the simulation system consisting of a silanol-capped amorphous silica slab coated (completely coverage) with multiple polymer strands of ADMPC in a particular solvent system composition as a starting point, prior to introducing the chiral analyte. Each parallel-antiparallel arrangement (*aaaa, aabb*, *abba*, *abab*) has to be prepared in this way. With every new solvent composition, the part of the flow chart bordered by red dashes has to be done over again.

and flavanone and thalidomide in methanol. For efficiency, we placed 5 molecules of each enantiomer in the simulation box and ran 200 ns simulations, taking steps to minimize stable dimerization of enantiomers, if any.

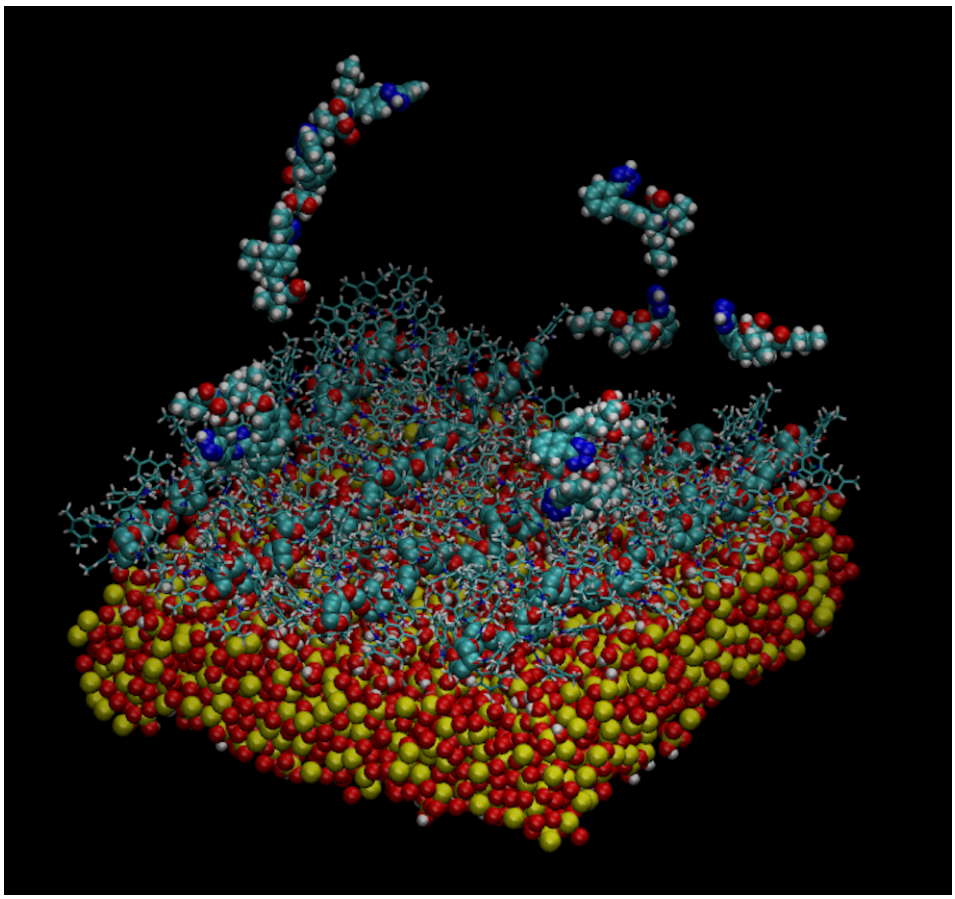

Figure 4. A snapshot of the simulation system. The amorphous silica slab is at the bottom of the simulation box, four 18-mer strands of ADMPC are held on the silanol-capped amorphous silica by van der Waals interactions. Enantiomers of benzoin are at the interface and in the bulk solvent. For clarity, the heptane and IPA molecules that constitute the solvent system are not displayed here. All atoms are permitted to move.

We noted any incidences of enantiomer interacting with more than one strand at a time, as well as any incidences of enantiomers sited in inter-strand regions for a succession of time frames. Methods of analysis of hydrogen-bonding lifetimes and the ring-ring interactions between the enantiomers and the ADMPC are used as described in Ref. [30]. We first analyzed results from each of four arrangements (*aaaa*), (*aabb*), (*abba*), and (*abab*) individually, to see whether parallel or antiparallel arrangements of

the helical polymer strands provide different results for the hydrogen-bonding statistics and the ring-ring interactions. Then, for an overall analysis, we combined the results together, resulting in equal contributions from parallel and anti-parallel arrangements, using the same six MD metrics that we had introduced in previous work. [29, 30]

Results presented in the lower part of Table S1 show that, as in the single strand model, different metrics give different results, but, at least in the case of benzoin and flavanone, the current model provides better consistency across all metrics as to which enantiomer elutes first, possibly due to the small number of possible donor-acceptor pairs compared to the cases of thalidomide and valsartan; the results for the latter could still be improved by longer MD runs. Unlike the results in the single strand model where maximum lifetimes provided the best correlations with experimental separation factors (probably due to insufficient sampling, despite three 100 ns runs, the averages were less reliable), it appears that of the 6 metrics, the overall average hydrogen bonding lifetimes provide the most consistent results.

We solved the problem of thalidomide. For thalidomide in methanol, the distributions of lifetimes clearly show longer lifetimes for the R relative to the S enantiomer, consistently for most of the donor-acceptor pairs. The single polymer strand model, [30] having missed two leading contributions to hydrogen bonding partners for the R enantiomer, failed to arrive at the correct answer that S thalidomide elutes first, found experimentally. We also solved the problem of valsartan. Our previous model did predict that R elutes first, having found S enantiomers forming many long-lived hydrogen bonds in 5 donor-acceptor pairs; however, the incidences of R enantiomers forming hydrogen bonds were far fewer, despite three 100 ns trajectories, leading to a ratio of S/R that is

orders of magnitude larger than the experimental separation factor of 1.29. [30] The present model found a large number of donor-acceptor pairs involved in hydrogen bonds between enantiomer and ADMPC that were previously missed. The current model provides a more complete sampling for both enantiomers, by a factor of 85. Furthermore, by providing the possibility of the valsartan molecule interacting with more than one strand at the same time, and by eliminating approaches from all directions around a polymer strand that are possible in single strand models, we capture the mode of interaction of valsartan with ADMPC on amorphous silica surface in hep/IPA in a more realistic way. The model is fully unrestrained, atomistically dynamic; no part of the system is restrained in any way. The dynamic behavior of a polymer with adjacent neighbors lying down on a silanol capped amorphous silica is very different from a free single polymer strand. The enantiomer approaches an interface, as it does in the real system, not a polymer strand that can be approached from all radial directions. Here the supramolecular chirality of the system is preserved in the regions between adjacent polymer strands, something that is totally missing from a single strand model. We had thought we would observe the effects of this by providing parallel and antiparallel arrangements, but we did not observe great differences between *aaaa*, *abab*, *abba*, and *aabb* arrangements for the four test analytes.

Incidences of an enantiomer interacting with two ADMPC chains simultaneously could not have been observed in a single strand model. We show in Fig. S2 in Supplementary Material a few snapshots demonstrating this phenomenon. Although such incidences do not dominate the overall results, they do occur many times during a simulation, and only the current model can permit such occurrences to be included;

single strand models miss these events entirely. In the examples shown in Fig. S2, the close interactions with two adjacent strands involve hydrophobic interactions with one strand, simultaneously with hydrogen bonding to the other strand, and such incidences are found in each of the four arrangements. In the particular close-up snapshot shown in Fig. S2, a valsartan ring forms a displaced face interaction with a phenyl ring of one ADMPC strand at the same time that the C=O2 of the valsartan gets close enough to the H-N of the adjacent ADMPC strand to form a hydrogen bond. For valsartan, such events appear to make a difference; and we expect this also to be the case with larger drug molecules.

7. What can MD simulations provide in terms of quantitative differential/discriminatory aspects for one enantiomer relative to the other?

MD can provide averages, and distributions, e.g., one- and two-body distribution functions, distributions of various geometric/structural features of diastereomers, of lifetimes of geometric structures, and free energy profiles, just to mention a few properties of a dynamic system.

7.1 Counts of H-bonds and distribution of hydrogen bonding lifetimes: Selector molecules such as polysaccharide-based CSPs have hydrogen bonding donor and acceptors; most drugs have a hydrogen-bonding donor and/or acceptor. Thus, it is common to have hydrogen bonding as the dominant interaction in the formation and stability of diastereomers. In such cases, it makes sense to consider counts of hydrogen-bonding events. In choosing our metrics, we go beyond that by including lifetimes in the analysis. Distributions of hydrogen-bonding lifetimes over the donor-acceptor pairs can be obtained, using standard geometric definitions of H-bonds,

namely, donor-acceptor distances less than 3.5 Å and angles greater than 135 °, which is not as strict as earlier geometric definitions. [80, 81]

Lifetimes of hydrogen-bonds between the enantiomers of the analyte and the CSP may be expected to correlate with retention times. From the snapshots taken every 2000 steps, say, the lifetime of a H-bond between a particular donor-acceptor pair is taken from the number of consecutive frames in which that H-bond is "on". [30] The distribution of lifetimes for each donor-acceptor pair can be informative. For example, Fig. S3 in Supplementary Material shows the distribution of hydrogen bonding lifetimes from MD simulations of valsartan with ADMPC in heptane/isopropanol (90/10). [31]

A close examination of the distribution of hydrogen bonding lifetimes for each of the drugs, such as those in Fig. S3 for valsartan, answers many questions sought by those who carry out molecular docking, such as, which is the most dominant donor acceptor pair(s) responsible for the long-lived enantiomer-selector interaction? are these also the ones responsible for selectivity or is it different for each enantiomer? In addition to the most dominant donor-acceptor pair for each enantiomer, however, we also find all the next level interactions that contribute to retention times, none are ignored in calculating the average hydrogen bonding lifetime. For those cases where there are only few H-bonding donor and acceptor pairs, such as benzoin and flavanone, the distribution plots are consistent and uniform in the higher incidences of H-bonding for one enantiomer compared to the other. We can then easily read from the plots which enantiomer should elute later. For those cases where there are multiple H-bonding donor and acceptor pairs, such as valsartan and thalidomide, which elutes last is not so easily discerned in the distribution plots; the enantiomers are hydrogen-bonding

differently with the ADMPC, one donor-acceptor pair may be particularly long-lived for one enantiomer but not for the other. In the overall average lifetimes metric, contributions from all pairs are appropriately weighted,

7.2 The role of ring-ring interactions : MD can provide the distribution of ring-ring orientations for analyte-selector interactions, and these distributions are descriptive of the dynamic approach to the recognition process. As an example, we examined the distribution of ring-ring orientations throughout a trajectory of benzoin where we have two distinct aromatic rings in the drug that can interact with the ADMPC in the single strand in solution as well as on the 4 polymer strands on a silica slab. Having a second ring helps to check on consistency of our description of what is going on in the molecular recognition. By considering only those ring orientations when the center-to-center distance is between 4 Å and 5 Å, we examine only close interactions of the analyte with the CSP interface.

Probability maps show that ring tilt angles range over the same values for both models. These maps inform on the ring-ring interactions assisting or discouraging close approach between donor-acceptor pairs. For both ring 1 and 2, S-benzoin has more incidences of center-to-center distances less than 4.4 A for both the single strand model and the multiple strands coated on silica. Thus, the ring-ring interactions also suggest that S benzoin elutes last.

7.3 Counts of diastereomeric complexes and lifetimes of diastereomer types: Some authors report differences between enantiomers by counting the number of van der Waals contacts between selector and analyte for each complex. In one example, they defined ‘strongly interacting complexes’ as those with greater than 10 vdW

contacts within the time interval, of an analyte which is an asymmetric pyrazoline interacting with cellulose tris (4-methyl benzoate), the time intervals corresponded to 1 ns vs 3.8 ns simulation times for the S and R enantiomers, respectively, that is, S spends more time in a strongly interacting complex than R does. [28] The experimental separation factor for this analyte in ethanol is a remarkable α = 73.2. In this example, cluster analyses of the so-defined strongly interacting complexes were also carried out. It is interesting to note that a very large fraction of the cluster types found were *identical to the starting docking poses*. [28] This could reflect distributions appropriate to free energy differences corresponding to a remarkable α = 73.2, or it could be at least partially a consequence of biasing via the starting configuration.

How to extract separation factors from MD simulations? This is not a trivial question. Cann et al. [38] have used an MD definition of separation factor: in Eqn (1). How does one find counts of “docked” versus “undocked” to use in Eqn (1). When H-bonding dominates the enantiomer-selector interactions and there is only one type of donor-acceptor pair, for example, a carbonyl oxygen of the selector and a hydroxyl of the analyte, [38] then with a geometric definition of the presence of a H-bond, every snapshot could provide the counts and the averages. However, using the idea of “docked” vs. “undocked” counting does not consider that even diastereomeric interactions that do not correspond to the global minimum can contribute to retention times for an enantiomer. When there are many possible donor-acceptor pair types, calculating separation factors from H-bonding counts in this way is no longer so simple and might even be misleading. For example, we have found that, for 10 different analytes and the selector 12-mer of ADMPC, in 3 different solvent systems, a count of

the number of frames in which a hydrogen bond was found between analyte and selector was not a particularly good metric to use for predicting separation factors.[30] In the case where several hydrogen bonding pairs could form, Cann et al. used the average percentages that an enantiomer has a H-bond to a chiral selector at any instant of time. [38]

For the polyproline selector, only H-bonding was used as a criterion for "docked" classification. Where both H-bonding and pi-pi stacking were considered significant, Cann et al. defined docked and undocked enantiomers in the following terms: [35] an analyte is considered docked when it simultaneously forms an H-bond and a π-π stack, and the presence of these interactions is determined by the application of the geometric criteria described above for a working definitions for a hydrogen bond and π-π stack. With these geometric definitions, the relative fractions of docked and undocked enantiomers can be obtained from a snapshot. In this way, they calculated separation factors for 10 different analytes. [35] For styrene oxide and stilbene oxide, they assumed a 3-point definition of when an enantiomer is docked with Whelk-O1 selector in n-hexane. [34] Here, there was only one H-bond to consider, but the counts of H-bonding were combined with counts of pi-pi stacking (counted when ring center-to-center distance is less than 4.6 Å between the phenyl ring of the epoxide and the phenanthryl or dinitrophenyl group of the selector), plus counts of a third contact, such as ring center-center distance between 4.6 Å and 6.5 Å). [34] Even in these simple cases, it is not clear how one should combine the information, whether assuming 2 points of contact, or always 3 points of contact defines "docked".

7.4 Free energy profile: The separation factor α can be calculated based on the difference of free energies for the R and S enantiomers

$$\Delta\Delta G = \Delta G_R - \Delta G_S = -RT \ln \alpha$$

Unfortunately, while both ΔG_R and ΔG_S are large (include non-selective interactions), $\Delta\Delta G$ will be small, especially when α is close to 1. In an MD simulation, it is possible to calculate the potential of mean force, as defined by Kirkwood in 1935. [82] The Potential of Mean Force of a system with N molecules is the potential that gives the average force over all the configurations of all the n+1, ..., N molecules acting on a particle *j* at any fixed configuration keeping fixed a set of molecules 1, ..., n:

$$-\nabla_j w^{(n)} = \frac{\int e^{-\beta V}(-\nabla_j V) dq_{n+1} \cdots dq_N}{\int e^{-\beta V} dq_{n+1} \cdots dq_N} \quad j = 1,2,\ldots,n \qquad (2)$$

where $\beta=1/k_BT$, the $\nabla_j w^{(n)}$ is the average force and therefore $w^{(n)}$ is the so-called Potential of Mean Force (PMF). A particular example would be $w^{(2)}(r_{12})$ that describes the interaction between two molecules held a fixed distance ***r*** when the remaining N-2 molecules are canonically averaged over all configurations. For example, in MD simulations of a ligand-coated nanoparticle crossing a lipid bilayer, we calculated the PMF, the free energy profile, for the 1, …., n atoms of a ligand-coated nanoparticle held at a fixed distance ***r*** along the path perpendicular to the bilayer surface, averaging over all of the configurations of the remaining atoms (solvent, lipids) in the simulation box. [83]

For simulations of chiral separation by a polymeric CSP, the complexity of the system is such that there is no clear choice of a reaction coordinate. However, for a cyclodextrin cup there is a well-defined reaction coordinate, the analyte goes from outside the cup, through it, to the other side, so the reaction coordinate may be taken as the path along the cup axis. Examples of PMF calculations are provided for R or S

flavanone molecule entering and leaving the β-cyclodextrin cup in a solvent system of methanol/water at equal-volume composition in the work by Li et al. [65]

The tethered cyclodextrin CSPs are shown in Fig. 2, where CSP2 is the normal configuration, that is, the wider mouth of the cup is exposed, and CSP1 is the reverse configuration, with the smaller mouth of the cup exposed. Li et al. calculated the PMF profiles for the reaction coordinate illustrated above each profile, the analyte goes into the cup in either orientation O1, that is, going in with the A phenyl ring in the lead. In orientation O2, the C ring is in the lead. In Fig. 5, two local minimum points and one energy barrier point appear along the reaction coordinate ξ in the process of complexation. The differences in the shapes of the PMF profiles for R vs. S are due to the chiral differences.

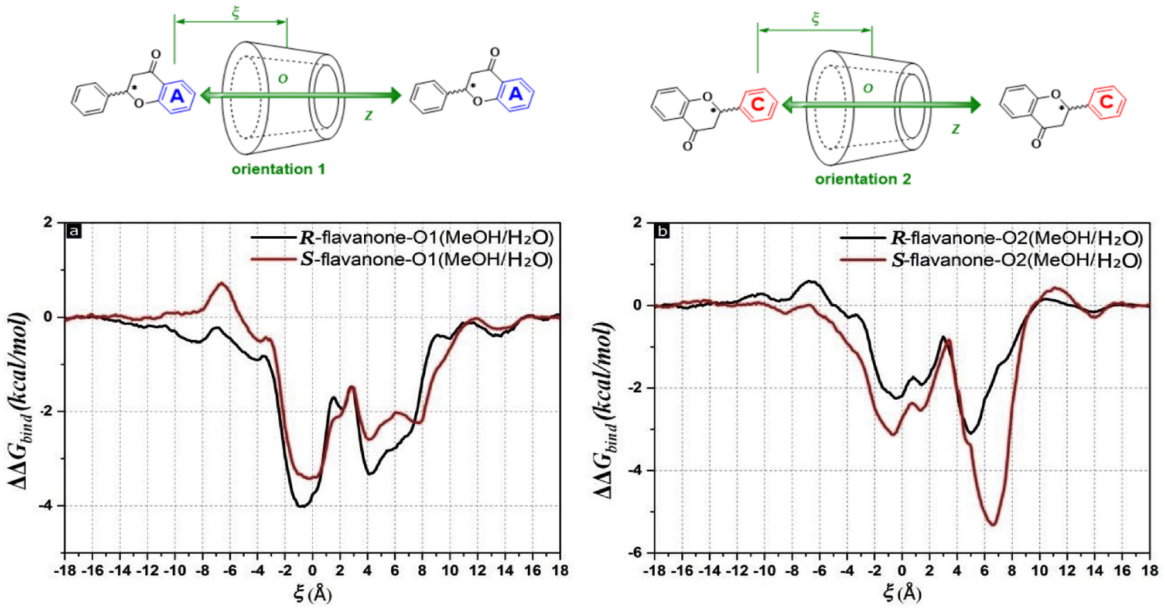

Figure 5. Free energy profiles for the inclusion of flavanone enantiomers into β-cyclodextrin in solvent MeOH/H_2O for the two cup orientations, consistent with the experimental results shown in Figure 2. Reproduced with permission from Ref. **65**.

First, let us look at the left figure in Fig. 5. It can be seen when the A ring of the flavanone enters the β-CD cavity, the free energy decreases rapidly. The first minimum energy point in the O1 orientation, the lowest free energy point, corresponds to ξ = - 0.8 Å for the R configuration and corresponds to ξ = - 0.2 Å for the S configuration. The snapshot at this lowest point shows the A ring completely centered in the β-CD cavity and the B ring is near the wider opening of β-CD. As the flavanone moves along further inside, there is an energy barrier. Further in, there is another minimum at ξ = 4.1 Å for both R and S, at which point the snapshot shows the C ring is in the center of the β-CD cavity and the B ring is near the narrower rim. In the right figure, the C ring of the flavanone first enters the β-CD cavity by the wider rim. As expected, there is a symmetry to the free energy profile, coming in through the wide mouth in the right figure is similar to leaving from the wide mouth in the left figure. This consistency in the PMF profiles is gratifying. When the phenyl A or C ring with hydrophobic property is located in the hydrophobic cavity of β-CD and the B ring with carbonyl group is located at the β-CD rim, the energy of the system reaches the local minimum.

In the above example, what can be obtained from the PMF profiles are the association free energies and the association equilibrium constants for the particular analyte (S or R flavanone) in the particular solvent: In O1 direction R has lower ΔG_{bind} (-0.98 kcal mol^{-1}) than S does (-0.61 kcal mol^{-1}). In O2 direction S has lower ΔG_{bind} (-1.83 kcal mol^{-1}) than R does (-0.27 kcal mol^{-1}). The difference in ΔG_{bind} between R and S in O1 is 0.37 kcal mol^{-1}, the difference in ΔG_{bind} between R and S in O2 is 1.56 kcal mol^{-1}, The larger difference in ΔG_{bind} between R and S corresponds to a larger separation factor in O2. Therefore, R flavanone should have a longer retention time, compared to

S, on reversed cup CSP1. Also, S flavanone should have a longer retention time on normal CSP2 compared to R, i.e., a reversal of elution order for flavanone in switching from CSP1 to CSP2. Experimental data shown in Fig. 2 do show the reversal in elution order, and also the greater separation in going from the reversed cup CSP1 to the normal cup CSP2. The PMF profiles from MD simulations provide the correct prediction and explanation for the experimental results. The association equilibrium constant for each enantiomer can be calculated from the ΔG_{bind} , and from these values for R and S, the separation factor can be calculated.

7.5 One-body and two-body distribution functions: One useful type of detailed information that can be obtained from MD simulations is the one-body distribution function (or density profile) for any component of the system, For example, from the distribution of solvent molecules at different regions of the interface, phenomena such as solvent partitioning, has been investigated by Cann et al., [33] in seeking to understand how it may be possible to change length and chemical composition of the tether, or composition of the solvent system in order to improve the selectivity of a CSP. [33, 36, 53] The one-body distribution maps for the S and R analytes in β-cyclodextrin provide similarly useful insights.[41] Such displays provide a better understanding of how the selectivity for R or S arises with the underivatized cyclodextrin, than does just the single global minimum structure from autodocking.

Two body-distribution functions $g(r_{12})$ (or radial distribution functions) provide the probability of finding any two atoms or groups at various distances, averaged over all configurations traversed by the trajectory. The first maximum in such distributions provide the most likely short distance between any two groups, for example an aromatic

ring on the analyte and a ring on the selector, [34] or any of the multitude of aromatic rings on a polymeric CSP, for example. The effect of substitution of bulky groups on the aromatic rings of the polymer can then be examined in MD simulations. Not only will such substitutions affect the ring-ring interactions, but as a result of such effects, ease of analyte approach to permit proximity of H-bonding donor and acceptor sites could be a concomitant consequence. This too can be displayed in the form of two-body distribution functions for donor-acceptor distances. Indeed, many such examples are provided by Cann et al., [33, 34, 37] and such radial distribution functions aid in understanding the separation process in the case of Whelk-O1 and proline-based CSPs. By making specific derivatives *in silico*, and looking at various distribution functions, it is easy to test for syntheses that may be profitably carried out to improve separation factors in various solvent conditions.

8. Future work

While in molecular docking methods one simply looks for the global minimum for each enantiomer interacting with the selector, there is no single configuration in MD, particularly when there are a multitude of possible local minima for the analyte with complex patterns of interactions having varying lifetimes and varying pathways of encounters with the CSP interface. We can continue to use MD to learn more accurate atomic-level details about the recognition process in each case, and we can very easily pose some questions that can be answered *in silico*, such as, if we were to make specific functional group substitutions in the selector, how would that affect the separation factor and which enantiomer elutes first an? As force fields improve and computing becomes ever more efficient, our MD results would improve in accuracy. We

could apply machine learning to MD simulations, attempt to discover essential features of chiral discrimination, and dependence on factors as yet unexplored.

CONFLICT OF INTEREST

The authors declare no competing financial interest.

ACKNOWLEDGMENT

This work was supported by The National Science Foundation (under Grant CBET 1545560).

REFERENCES

[1] Rossi D, Tarantino M, Rossino G, Rui M, Juza M, Collina S. Approaches for multi-gram scale isolation of enantiomers for drug discovery. *Expert Opinion Drug Discovery*. 2017;12:1253-1269.

[2] Ward TJ, Ward KD. Chiral separations by high-performance liquid chromatography. In: Encyclopedia of analytical chemistry. New York: John Wiley, 2012.

[3] Evertsson E, Rönnberg J, Stålring J, Thunberg L. A hierarchical screening approach to enantiomeric separation. *Chirality*. 2017;29:202-212.

[4] Klein-Júnior LC, Mangelings D, Vander Heyden Y. Experimental design methodologies for the optimization of chiral separations: An overview. In: Scriba GKE. Chiral Separations Methods and Protocols. Vol. 1985 of Methods in Molecular Biology Series. New York: Humana, 2019:453-478.

[5] Tachibana K, Ohnishi A. Reversed-phase liquid chromatographic separation of enantiomers on polysaccharide type chiral stationary phases. *J. Chromatogr. A*. 2001;906:127–154.

[6] Felinger A. Molecular dynamic theories in chromatography. *J. Chromatogr. A*. 2008;1184:20-41.

[7] Pasti L, Cavazzini A, Nassi M, Dondi F. Dynamic chromatography: A stochastic approach. *J. Chromatogr. A*. 2010;1217:1000–1009.

[8] Pasti L, Marchetti N, Guzzinati R, Catani M, Bosi V, Dondi F, Sepsey A, Felinger A, Cavazzini A. Microscopic models of liquid chromatography: From ensemble averaged information to resolution of fundamental viewpoint at single-molecule level. *Trends Anal. Chem*. 2016;81:63–68.

[9] Davankov VA. The nature of chiral recognition: Is it a three-point interaction?, *Chirality*. 1997;9:99-102.

[10] Easson LH, Stedman E. Studies on the relationship between chemical constitution and physiological action: Molecular dissymmetry and physiological activity. *Biochem. J*. 1933;27:1257-1266.

[11] Lipkowitz KB. Atomistic modeling of enantioselection in chromatography. *J. Chromatogr. A*. 2001;906:417–442.

[12] Lindsey RK, Rafferty JL, Eggimann BL, Siepmann JI, Schure MR. Molecular simulation studies of reversed-phase liquid chromatography. *J. Chromatogr. A*. 2013;1287:60–82.

[13] Pirkle WH, Pochapsky TC. Considerations of chiral recognition relevant to the liquid chromatography separation of enantiomers. *Chem. Rev*. 1989;89:347–362.

[14] Topiol S, Sabio M. Interactions between eight centers are required for chiral recognition. *J. Am. Chem. Soc*. 1989;111:4109–4110.

[15] Bentley R. Diastereoisomerism, contact points, and chiral selectivity: a four-site saga. *Arch. Biochem. Biophys*. 2003;414:1-12.

[16] Topiol S. A general criterion for molecular recognition: Implications for chiral interactions. *Chirality*. 1989;1:69–79.

[17] Lämmerhofer M. Chiral recognition by enantioselective liquid chromatography: Mechanisms and modern chiral stationary phases. *J. Chromatogr. A*. 2010;1217:814-856.

[18] Morris GM, Goodsell DS, Halliday RS, Huey R, Hart WE, Belew RK, Olson AJ. Automated docking using a Lamarckian genetic algorithm and an empirical binding free energy function. *J. Comput. Chem*. 1998;19:1639–1662.

[19] Morris GM, Huey R, Lindstrom W, Sanner MF, Belew RK, Goodsell DS, Olson AJ. AutoDock4 and AutoDockTools4: Automated docking with selective receptor flexibility. *J. Comput. Chem*. 2009;30:2785–2791.

[20] Alcaro S, Gasparrini F, Incani O, Mecucci S, Misiti D, Pierini M, Villani C. A "Quasi-flexible" automatic docking processing for studying stereoselective recognition mechanisms. Part I. Protocol validation. *J. Comput. Chem.* 2000;21:515–530.

[21] Barfeii H, Garkani-Nejad Z, Saheb V. Investigation of the mechanism of enantioseparation of some drug compounds by considering the mobile phase in HPLC by molecular dynamics simulation. *J. Mol. Model*. 2019;25:297.

[22] Dou X, Su X, Wang Y, Chen Y, Shen W. Studies on pidotimod enantiomers with Chiralpak-IA: crystal structure, thermodynamic parameters and molecular docking. *Chirality*. 2015;27:802–808.

[23] Ali I, Lone MN, Suhail M, Al-Othman ZA, Alwarthan A. Enantiomeric resolution and simulation studies of four enantiomers of 5-bromo-3-ethyl-3-(4- nitrophenyl)- piperidine-2,6-dione on a Chiralpak IA column. *RSC Adv*. 2016;6:14372-14380.

[24] Ali I, Haque A, Al-Othman ZA, Al-Warthan A, Asnin L. Stereoselective interactions of chiral dipeptides on amylose based chiral stationary phases. *Sci. China Chem*. 2015;58:519–525.

[25] Rossi D, Nasti R, Collina S, Mazzeo G, Ghidinelli S, Longhi G, Memo M, Abbate S. The role of chirality in a set of key intermediates of pharmaceutical interest, 3-aryl-substituted-γ-butyrolactones, evidenced by chiral HPLC separation and by chiroptical spectroscopies. *J. Pharm. Biomed. Anal*. 2017;144:41–51.

[26] Pisani L, Rullo M, Catto M, de Candia M, Carrieri A, Cellamare S, Altomare CD. Structure–property relationship study of the HPLC enantioselective retention of neuroprotective 7-(1-alkylpiperidin-3-yl)methoxycoumarin derivatives on an amylose-based chiral stationary phase. *J. Sep. Sci*. 2018;41:1376–1384.

[27] Xiong F, Yang BB, Zhang J, Li L. Enantioseparation, stereochemical assignment and chiral recognition mechanism of sulfoxide-containing drugs. *Molecules*. 2018;23:2680.

[28] Alcaro S, Bolasco A, Cirilli R, Ferretti R, Fioravanti R, Ortuso F. Computer-aided molecular design of asymmetric pyrazole derivatives with exceptional enantioselective recognition toward the chiralcel OJ-H stationary phase. *J. Chem. Inf. Model*. 2012;52:649-654.

[29] Zhao BW, Oroskar PA, Wang XY, House D, Oroskar A, Oroskar A, Jameson CJ, Murad S. The composition of the mobile phase affects the dynamic chiral recognition of drug molecules by the chiral stationary phase. *Langmuir*. 2017;33:11246-11256.

[30] Wang XY, House D, Oroskar A, Oroskar A, Jameson CJ, Murad S. Molecular dynamics simulations of the chiral recognition mechanism for a polysaccharide chiral stationary phase in enantiomeric chromatographic separations. *Mol. Phys*. 2019;117:3569-3588.

[31] Wang XY, Jameson CJ, Murad S. Modeling enantiomeric separations as an interfacial process using amylose tris(3,5-dimethylphenyl carbamate) (ADMPC) polymers coated on amorphous silica. *Langmuir*. 2020;36:1113-1124.

[32] Nita S, Cann NM. Solvation of phenylglycine- and leucine-derived chiral stationary phases: molecular dynamics simulation study. *J. Phys. Chem B*. 2008;112:13022-13037.

[33] Zhao CF, Cann NM. Solvation of the Whelk-O1 chiral stationary phase: A molecular dynamics study. *J. Chromatogr. A*. 2006;1131:110-129.

[34] Zhao CF, Cann NM. The docking of chiral epoxides on the Whelk-O1 stationary phase: a molecular dynamics study. *J Chromatogr A*. 2007;1149:197-218.

[35] Zhao CF, Cann NM. Molecular dynamics study of chiral recognition for the whelk-o1 chiral stationary phase. *Anal. Chem*. 2008;80:2426-2438.

[36] Zhao CF, Diemert S, Cann NM. Rational optimization of the Whelk-O1 chiral stationary phase using molecular dynamics simulations. *J. Chromatogr. A*. 2009;1216:5968-5978.

[37] Ashtari M, Cann NM. Proline-based chiral stationary phases: A molecular dynamics study of the interfacial structure. *J. Chromatogr. A*. 2011;1218:6331-6347.

[38] Ashtari M, Cann NM. The docking of chiral analytes on proline-based chiral stationary phases: A molecular dynamics study of selectivity. *J. Chromatogr. A*. 2015;1409:89-107.

[39] Arjumand R, Ebralidze II, Ashtari M, Stryuk J, Cann NM, Horton JH. Chiral discrimination of a proline-based stationary phase: adhesion forces and calculated selectivity factors. *J. Phys. Chem. C*. 2013;117:4131-4140.

[40] Alvira E. Influence of solvent polarity on the separation of leucine enantiomers by beta-cyclodextrin: a molecular mechanics and dynamics simulation. *Tetrah. Asymm*. 2017;28:1414-1422.

[41] Alvira E. Molecular simulation of the separation of isoleucine enantiomers by β-cyclodextrin. *Molecules*. 2019;24:1021.

[42] Melani F, Pasquini B, Caprini C, Gotti R, Orlandini S, Furlanetto S. Combination of capillary electrophoresis, molecular modeling and NMR to study the enantioselective complexation of sulpiride with double cyclodextrin systems. *J. Pharm. Biomed. Anal*. 2015;114:265–271.

[43] Pasquini B, Melani F, Caprini C, Del Bubba M, Pinzauti S, Orlandini S, Furlanetto S. Combined approach using capillary electrophoresis, NMR and molecular modeling for ambrisentan related substances analysis: Investigation of intermolecular affinities, complexation and separation mechanism. *J. Pharm. Biomed. Anal*. 2017;144:220–229.

[44] Hu GX, Huang M, Luo C, Wang Q, Zou J. Interactions between pyrazole derived enantiomers and Chiralcel OJ: Prediction of enantiomer absolute configurations and elution order by molecular dynamics simulations. *J. Molec. Graph. Model*. 2016;66:123-132.

[45] Ye YK, Bai S, Vyas S, Wirth MJ. NMR and computational studies of chiral discrimination by amylose tris(3,5-dimethylphenylcarbamate). *J. Phys. Chem. B*. 2007;111:1189-1198.

[46] Dodziuk H, Lukin O. Modelling of molecular and chiral recognition by cyclodextrins. Is it reliable? Part 2. Molecular dynamics calculations in vacuum pertaining to the selective complexation of decalins by beta-cyclodextrin. *Polish J. Chem*. 2000;74:997-1001.

[47] Kasat RB, Franses EI, Wang NHL. Experimental and computational studies of enantioseparation of structurally similar chiral compounds on amylose tris(3,5-dimethylphenylcarbamate). *Chirality*. 2010;22:565-579.

[48] Li Y, Liu D, Wang P, Zhou Z. Computational study of enantioseparation by amylose tris(3,5-dimethylphenylcarbamate)-based chiral stationary phase. *J. Sep. Sci*. 2010;33:3245-3255.

[49] Wang T, Wenslow, Jr. RM. Effects of alcohol mobile-phase modifiers on the structure and chiral selectivity of amylose tris(3,5-dimethylphenylcarbamate) chiral stationary phase. *J. Chromatogr. A*. 2003;1015:99–110.

[50] Scriba GKE. Chiral recognition mechanisms in analytical separation sciences. *Chromatographia*. 2012;75:815-838.

[51] Scriba GKE. Chiral recognition in separation science – an update. *J. Chromatogr. A*. 2016;1467:56–78.

[52] Nita S, Cann NM. Structure, selectivity, and solvation of a model chiral stationary phase. *J. Phys. Chem B*. 2004;108:3512-3522.

[53] Nita S, Cann NM. Solvation of the N-(1-phenylethyl)-N '-3-(triethoxysilyl)propyl-urea chiral stationary phase in mixed alcohol/water solvents. *J. Phys. Chem B*. 2006;110:9511-9519.

[54] Hall K, Ashtari M, Cann NM. On simulations of complex interfaces: Molecular dynamics simulations of stationary phases. *J. Chem. Phys*. 2012;136:114705.

[55] Ashtari M, Cann NM. Poly-proline-based chiral stationary phases: A molecular dynamics study of triproline, tetraproline, pentaproline and hexaproline interfaces. *J. Chromatogr. A*. 2012;1265:70-87.

[56] Varga G, Tarkanyi G, Nemeth K, Ivanyi R, Jicsinszky L, Tőke O, Visy J, Szente L, Szemán J, Simonyi M. Chiral separation by a monofunctionalized cyclodextrin derivative: from selector to permethyl-beta-cyclodextrin bonded stationary phase. *J. Pharm. Biomed. Anal*. 2010;51:84–89.

[57] Xiao Y, Ng SC, Tan TT, Wang Y. Recent development of cyclodextrin chiral stationary phases and their applications in chromatography. *J. Chromatogr. A*. 2012;1269:52–68.

[58] Tang WH, Ng SC, Sun D.P. Modified cyclodextrins for chiral separation. Berlin: Springer-Verlag, 2013.

[59] Zhou J, Tang J, Tang W. Recent development of cationic cyclodextrins for chiral separation. *Trends Anal. Chem*. 2015;65:22–29.

[60] Li XX, Wang Y. HPLC Enantioseparation on cyclodextrin-based chiral stationary phases. In: Scriba GKE. Chiral separations. Vol. 1985 of Methods in Molecular Biology Series. New York: Humana, 2019.

[61] Das O, Ghate VM, Lewis SA. Utility of sulfobutyl ether beta-cyclodextrin inclusion complexes in drug delivery: A review. *Indian J. Pharm. Sci*. 2019;81:589-600.

[62] Köhler JEH, Hohla M, Richters M, König WA. Cyclodextrin derivatives as chiral selectors - investigation of the interaction with (R,S)-methyl-2-chloropropionate by enantioselective

gas-chromatography, NMR-spectroscopy, and molecular-dynamics simulation. *Angew. Chemie, Int. Ed*. 1992;31:319-320.

[63] Uccello-Barretta G, Schurig V, Balzano F, Vanni L, Aiello F, Mori M, Ghirga F. Synergistic effects of trace amounts of water in the enantiodiscrimination processes by lipodex e: a spectroscopic and computational investigation. *Chirality*. 2015;27:95-103.

[64] Škvára J, Nezbeda I, Izák P. Molecular dynamics study of racemic mixtures. II. Temperature dependence of the separation of ibuprofen racemic mixture with β-cyclodextrin in methanol solvent. *J. Molec. Liq*. 2020;302:112575.

[65] Li XX, Yao XB, Xiao Y, Wang Y. Enantioseparation of single layer native cyclodextrin chiral stationary phases: Effect of cyclodextrin orientation and a modeling study. *Anal. Chim. Acta*. 2017;990:174-184.

[66] Felix G, Berthod A. Commercial chiral stationary phases for the separations of clinical racemic drugs Part II: From dermatologicals to sensory organ and various drugs. *Sep. Purific. Rev*. 2008;37:1- 227.

[67] Felix G, Berthod A. Commercial chiral stationary phases for the separations of clinical racemic drugs Part III: Supercritical fluid chromatographic separations. *Sep.Purific. Rev*. 2008;37:229-301.

[68] Chankvetadze B, Kartozia I, Yamamoto C, Okamoto Y. Comparative enantioseparation of selected chiral drugs on four different polysaccharide-type chiral stationary phases using polar organic mobile phases. *J. Pharm. Biomed. Anal*. 2002;27:467-478.

[69] Chankvetadze B, Chankvetadze L, Sidamonidze S, Yashima E, Okamoto Y. High performance liquid chromatography enantioseparation of chiral pharmaceuticals using tris(chloro-methylphenylcarbamate)s of cellulose. *J. Pharm. Biomed. Anal*. 1996;14:1295-1303.

[70] Chankvetadze B. Polysaccharide-based chiral stationary phases for enantioseparations by high-performance liquid chromatography: An overview. In: Scriba GKE. Chiral separations methods and protocols. Vol. 1985 of Methods in Molecular Biology series. New York: Humana, 2019: 93-126.

[71] Ye YK. Chiral discrimination study for polysaccharide-based chiral stationary phases. In: Ahuja S. Chiral separation methods for pharmaceutical and biotechnological products. New York: Wiley, 2010:147-191.

[72] Ikai T, Okamoto Y. Structure control of polysaccharide derivatives for efficient separation of enantiomers by chromatography. *Chem. Rev*. 2009;109:6077-6101.

[73] Hellriegel C, Skogsberg U, Albert K, Lämmerhofer M, Maier NM, Lindner W. Characterization of a chiral stationary phase by HR/MAS NMR spectroscopy and investigation of enantioselective interaction with chiral ligates by transferred NOE. *J. Am. Chem. Soc.* 2004;126:3809-3816.

[74] Yamamoto C, Yashima E, Okamoto Y. Structural analysis of amylose tris(3,5-dimethylphenylcarbamate) by NMR relevant to its chiral recognition mechanism in HPLC. *J. Am. Chem. Soc*. 2002;124:12583-12589.

[75] Ma S, Shen S, Lee H, Eriksson M, Zeng X, Xu J, Fandrick K, Yee N, Senanayake C, Grinberg N. Mechanistic studies on the chiral recognition of polysaccharide-based chiral stationary phases using liquid chromatography and vibrational circular dichroism: reversal of elution order of N-substituted alpha-methyl phenylalanine esters. *J. Chromatogr. A*. 2009;1216:3784-3793.

[76] Wenslow RM, Wang T. Solid-state NMR characterization of amylose tris(3,5-dimethylphenylcarbamate) chiral stationary-phase structure as a function of mobile-phase composition. *Anal. Chem*. 2001;73:4190−4195.

[77] Kasat RB, Wang NHL, Franses EI. Effects of backbone and side chain on the molecular environments of chiral cavities in polysaccharide-based biopolymers. *Biomacromolecules*. 2007;8:1676-1685.

[78] Ye YK, Bai S, Vyas S, Wirth MJ. NMR and computational studies of chiral discrimination by amylose tris(3,5-dimethylphenylcarbamate). *J. Phys. Chem. B*. 2007;111:1189-1198.

[79] Ramachandran GN, Ramakrishnan C, Sasisekharan V. Stereochemistry of polypeptide chain configurations. *J. Molec. Biol*. 1963;7:95–9.

[80] Luzar A, Chandler D. Hydrogen-bond kinetics in liquid water. *Nature*. 1996;379:55-57.

[81] Levitt M, Sharon R. Accurate simulation of protein dynamics in solution. *Proc. Natl. Acad. Sci. U.S.A*. 1988;85:7557-7561.

[82] Kirkwood JG. Statistical mechanics of fluid mixtures. *J. Chem. Phys*. 1935;3:300-313.

[83] Song B, Yuan HJ, Jameson CJ, Murad S. Permeation of nanocrystals across lipid membranes. *Mol. Phys*. 2011;109:1511-1526.